Visual Abstract

PVC failure modelling through experimental and digital image correlation measurements

Zekriti Najat, Majid Fatima
Laboratory of Nuclear, Atomic, Molecular, Mechanical and Energetic Physics, University Chouaib Doukkali, El jadida, Morocco
najat.ze@hotmail.fr, majidfatima9@gmail.com

Rhanim Rajaa
Laboratory Study of Advanced Materials and Application, University Moulay Ismail, Meknes, Morocco
rajaaarhanim@gmail.com

Mrani Ibrahim, Rhanim Hassan
Laboratory of Nuclear, Atomic, Molecular, Mechanical and Energetic Physics, University Chouaib Doukkali, El jadida, Morocco
ibmrani@gmail.com, rhanimhassan@hotmail.com

ABSTRACT. This paper analyses industrial PVC sheets structural integrity assessment widely used for different ranges of industrial applications. We investigated combined approaches focused on fracture toughness assessment to predict PVC mechanical behavior against failure. We ran a series of tests on tensile and single-edge notched samples at various crosshead speeds on a tensile test machine. PVC sheets' stress intensity factors were evaluated using both theoretical and experimental approaches to model crack growth. In the experimental procedure, we used the digital image correlation (DIC) method. We also developed a semi-empirical model to predict crack length over time. Furthermore, we proposed that the crack growth rate and stress intensity factor were satisfactorily correlated at all crosshead speeds and that the crack growth rate could be represented using a power-law model. In pre-cracked PVC specimens, the results showed that crack growth appears to be influenced by crosshead speed.

KEYWORDS. Crack growth; stress intensity factor; strain rates; DIC; PVC.

OPEN ACCESS

Citation: Zekriti, N., Majid, F., Rajaa, R., Mrani, I., Rhanim, H., PVC failure modelling through experimental and digital image correlation measurements, Frattura ed Integrità Strutturale, 60 (2022) 488-503.

Received: 17.12.2021
Accepted: 16.03.2022
Online first: 22.03.2022
Published: 01.04.2022

INTRODUCTION

Due to cracks or crack-like flaws in most engineering structures and components produced during the manufacturing process or developed at the initial stage of its service life, fracture mechanics, a branch of mechanics concerned with crack propagation in materials, has advanced. Linear elastic fracture mechanics (LEFM) is a technique for determining the conditions under which a crack grows by determining the cracked part's linear elastic stress [1].

Many authors have highlighted the importance of failure studies so that future designs can be adapted to anticipate and prevent similar failures[2,3].
However, it affords the required descriptive and analytical basis to identify crack growth rates and their implementation in concrete engineering issues [4–8].
The formation of geometric discontinuities such as cracks makes thermoplastic materials susceptible to premature failure depending on service conditions. The detection of these defects is complex, and their growth may result in catastrophic accidents. As a result, monitoring and maintenance are critical for maintaining high integrity, reliability, plant efficiency, and sophisticated maintenance concept adjustments based on experimental research.
Over the last decade, the use of plastic in piping and building construction has soared. Window, exterior cladding, patio doors, architraves, and ranch fencing are examples of these applications. Polyvinyl Chloride (PVC) is the most popular material; it was first used in manufacturing before World War II and has been a significant contributor to the plastics industry. PVC production was first registered in 1835 by Regnault and was patented in 1912 by German chemist August Wilhelm von Hofmann. From 1986 to today, rigid PVC extrusion has dominated [9,10].
On the other hand, over the last century, the number of studies on PVC has increased considerably, based on PVC microstructure and mechanical characterization [11–16] as well as the study of fracture and fatigue involving life prediction [17–21]; furthermore, crack growth behavior has been at the heart of the understanding of PVC behavior[22–24].
The value of developing a model to explain the crack growth rate has been demonstrated in numerous studies of fatigue crack growth damage[25]. Through Paris and Erdogan [26] which postulated that the rate of crack growth is controlled primarily by the change in the stress intensity factor, the Paris law was proposed as following:

$$\frac{da}{dN} = C(\Delta K)^m \tag{1}$$

Nevertheless, few authors have drawn on any systematic research into fracture crack growth as a crosshead speed function [27–30]. As a result, developing a general model for fracturing and describing the crack growth rate is challenging.
As a result, in this study, we propose an empirical model based on a simple power-law [31,32] to address the following fundamental questions: Does it matter if a crack was detected during an inspection? What is the estimated duration of this crack's existence? What is the maximum crack size that can be tolerated? What are the characteristics of PVC crack propagation at various crosshead speeds?
The most commonly used technique for determining crack length is digital image correlation (DIC) [33–35], which is a low-cost and simple technique. Sutton and Chu proposed DIC [36–38], a non-contact optical method for measuring kinematic fields, in the 1980s. This technique allows for the measurement of displacement and deformation fields at all points on the surface of the work-piece, on the principle of comparing two images taken at different loading stages, one referred to as a reference and the other as the deformed state [39,40].
This paper aims to assess and model the crack growth behavior of PVC. Single edge notched tensile (SENT) specimens are made from industrial PVC sheets and classified into three groups. All specimens have been pre-cracked artificially. The effect of test conditions, precisely crosshead speed (5,10, 100mm/min), on PVC and crack growth rate, mechanical properties are investigated under static tests throughout this study. The LEFM theory can be used to calculate the critical stress intensity factor of rigid PVC (KIc). The Ncorr program is used to evaluate the crack length using the DIC method. An empirical model between crack length and life fraction has been suggested, and a model has been proposed using a simple power-law assuming an intrinsic parameter of the PVC after an in-depth study of crack growth behavior. Finally, an optical microscopy is used for morphological examination of damaged zones of fractured SENT specimens.

EXPERIMENTAL AND METHODS

Preparation of tensile specimens

Polyvinyl chloride (PVC), a synthetic resin made by polymerizing vinyl chloride, was used in this work. It is made from two different starting materials: 57% salt (NaCl) and 43% hydrocarbon feedstocks.
In accordance with ASTM D638 standard, the Single Edge Notched Tensile specimens were made from compression-molded plates, laser-cut, and then mechanically pre-cracked with a razor blade, with dimensions of 150x19x3mm3 Fig. 1 Uniaxial tensile tests were performed with three crosshead speeds of 5 mm/min, 10 mm/min, and 100 mm/min using a tensile test machine, MTS Fig. 2, with the technical characteristics described in Tab. 1. A total of 15 specimens were produced and divided into three subgroups of five specimens each, using simple random sampling:

- Group I - at crosshead speed of 5 mm/min;
- Group II - at crosshead speed of 10 mm/min;
- Group III - at crosshead speed of 100 mm/min.

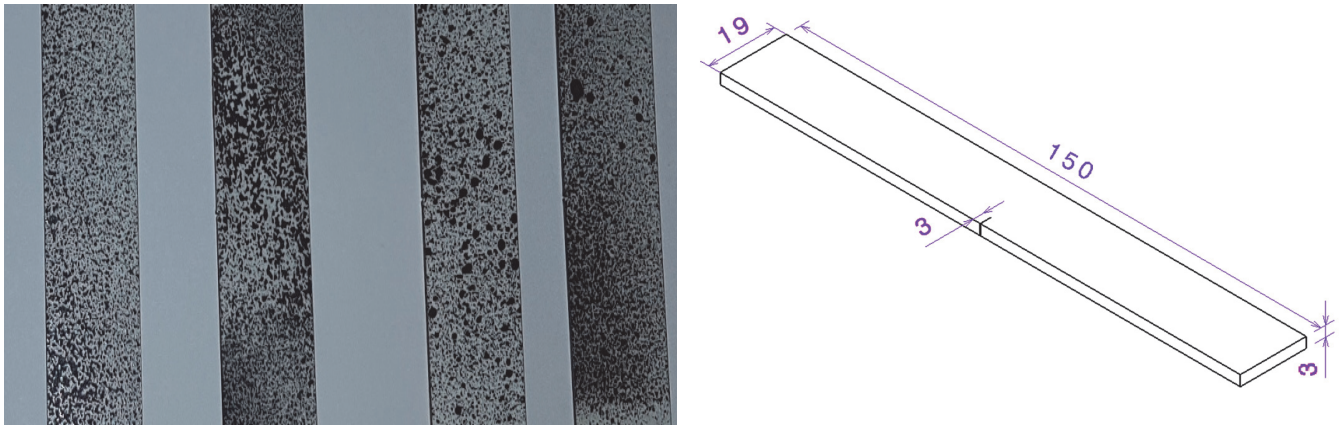

Figure 1: Dimensions of PVC beams.

MTS	
Capacity	50KN
Accuracy of displacement	Class ±0.5%
Maximum test speed	1020mm/min
Minimum test speed	0.005mm/min
Resolution position control	0.00006mm

Table 1: Technical characteristics of the tensile test machine.

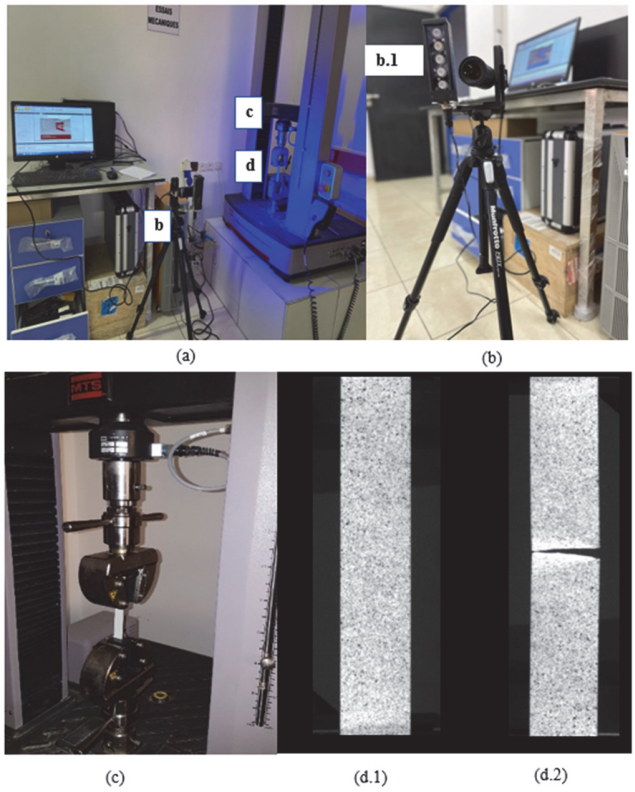

Figure 2: (a)Tensile testing system; (b) DIC system; (b.1) LED Light source; (c)MTS testing machine; (d.1) dumbbell specimen before deformation; (d.2) dumbbell specimen after rupture.

Furthermore, random patterns were painted on each SENT's face with black paint to create the speckle pattern, which was differentiated from discontinuous displacement fields using the DIC technique. The digital images were captured using an IDS camera UI-3880CP Fig.2, whose specifications are described in Tab. 2. In order to ensure that the conditions for taking pictures during the experiments were consistent for the cameras, the experimental field was lighted by bar light essential 15 blue LEDS +/- 25° with polarizer Fig.2. They constituted the part of the measuring equipment in the DIC method. The light was chosen and supplied by the manufacturer of the camera in such a way that a uniform intensity over the entire lighted surface of the specimen was reached. Fig. 3 depicts a block diagram of the measurement process. And also, to further understand the effect of crosshead speed on the fracture mechanical response, the surface of the fractured SENT specimens was examined using an optical microscope (Fig. 4).

IDS	
Full resolution	3088 x 2076 Pixel
Optical surface	7.410 mm x 4.980 mm
Pixel size	2.4 µm
Pixel frequency range	20 MHz - 474 MHz

Table 2: Technical characteristics of the IDS camera UI-3880CP.

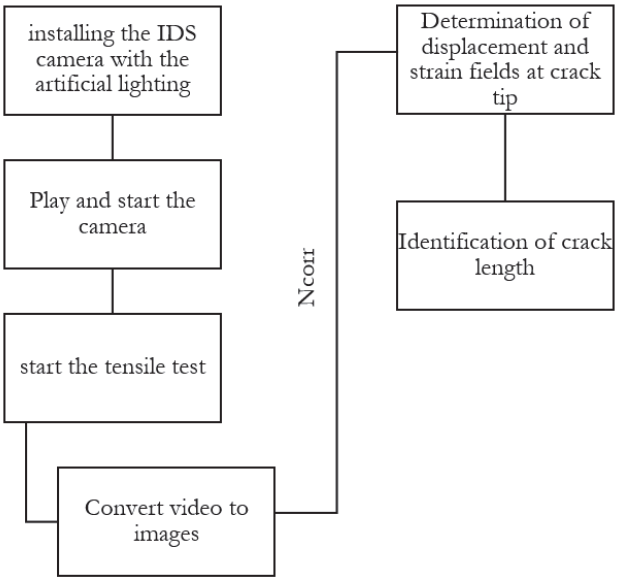

Figure 3: The block diagram of the proposed measuring method.

Figure 4: Optical microscope.

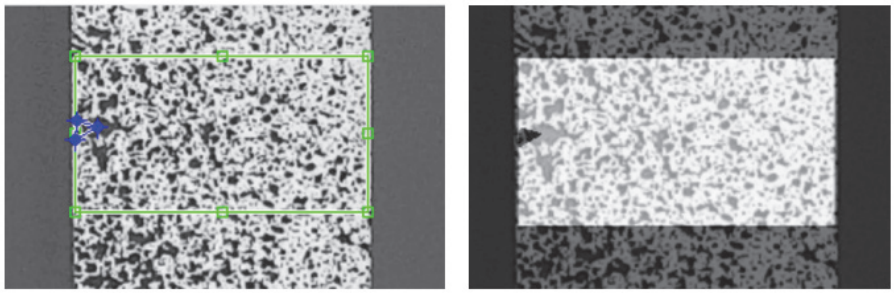

(a) (b)

Figure 5: (a) Drawing of ROI; (b) ROI preview.

DIGITAL IMAGE CORRELATION

DIC aims to evaluate the displacement field within a "Region Of Interest" (ROI) for a deformed sample Fig. 5. The DIC method divides the reference image into small subsections, referred to as subsets, and defines their corresponding positions in the current image.
Modern algorithms proposed in the literature [41–45] are used to develop open-source software based on a 2D subset in this context (Ncorr) [46–48].

Identification of crack length

During the experiment, a precise measurement of the crack length is needed to assess the crack growth rate. We used the Ncorr software to investigate the crack length in our samples.
The algorithm used to locate the crack tip in the SENT test samples assumes that the stress at this position reaches its peak once the crack tip zone gives way. Thus, the crack tip location is determined by calculating the maximum axial strain Eyy values in the loading direction y.
To better understand how to evaluate discontinuous displacement fields in Ncorr, we first developed the ROI for the running image rather than the reference image, ran DIC, and then converted the Eulerian to the Lagrangian algorithm with subset truncation in Ncorr to acquire data in a diameter subset closer to the crack tip area.
Ncorr makes use of Green-Lagrangian strains, which are generated using the following three displacement gradients:

$$E_{xx} = \frac{1}{2}\left(2\frac{\partial u}{\partial x} + \left(\frac{\partial u}{\partial x}\right)^2 + \left(\frac{\partial v}{\partial x}\right)^2\right) \tag{2}$$

$$E_{xy} = \frac{1}{2}\left(\frac{\partial u}{\partial y} + \frac{\partial v}{\partial x} + \frac{\partial u \partial u}{\partial x \partial y} + \frac{\partial v \partial v}{\partial x \partial y}\right) \tag{3}$$

$$E_{yy} = \frac{1}{2}\left(2\frac{\partial u}{\partial y} + \left(\frac{\partial u}{\partial y}\right)^2 + \left(\frac{\partial v}{\partial y}\right)^2\right) \tag{4}$$

Stress intensity factor

The establishment of experimental data and the determination of the stress field and corresponding deformations enable a decision to be made on the kinetics of defect propagation and their critical size, beyond which the unstable break will be triggered for a given stress. According to Irwin [49–51], determining the stress intensity factors KI, KII, and KIII in mode I, II, or III characterize the stress field's entire spatial singularity is the key to solving a crack problem.
Consider a crack with a straight edge, such as a planar crack. This holds for a discontinuity of zero natural stresses and discontinuous displacement on both sides of the crack's lips.
The most studied mode is the opening mode, which is considered the most dangerous. The stress and displacement fields in mode I are given as follows according to the classical theory of elasticity:

Stress

$$\sigma_{xx} = \frac{K_I}{\sqrt{2\pi r}}\cos\frac{\theta}{2}\left(1 - \sin\frac{\theta}{2}\sin\frac{3\theta}{2}\right) \tag{5}$$

$$\sigma_{yy} = \frac{K_I}{\sqrt{2\pi r}}\cos\frac{\theta}{2}\left(1 + \sin\frac{\theta}{2}\sin\frac{3\theta}{2}\right) \tag{6}$$

$$\sigma_{xy} = \frac{K_I}{\sqrt{2\pi r}}\cos\frac{\theta}{2}\left(\sin\frac{\theta}{2}\sin\frac{3\theta}{2}\right) \tag{7}$$

$$\sigma_{zz} = \nu(\sigma_{xx} + \sigma_{yy}) \quad \text{For plane strain} \tag{8}$$

$$\sigma_{zz} = 0 \quad \text{For plane stress} \tag{9}$$

Displacement

$$u_x = \frac{K_I}{2\mu}\sqrt{\frac{r}{2\pi}}\cos\frac{\theta}{2}(\kappa - 1 + 2\sin^2\frac{\theta}{2}) \tag{10}$$

$$u_y = \frac{K_I}{2\mu}\sqrt{\frac{r}{2\pi}}\sin\frac{\theta}{2}(\kappa + 1 - 2\cos^2\frac{\theta}{2}) \tag{11}$$

$$\kappa = 3 - 4\nu \quad \text{Plane strain} \tag{12}$$

$$\kappa = \frac{3-\nu}{1-\nu} \quad \text{Plane stress} \tag{13}$$

The stress intensity factor is a function of both loading and geometry to describe the stress distribution at the crack edge, as shown by relations 5, 6, 7. The form of stresses at the crack tip are known to exhibit a characteristic inverse square-root dependence on r when using polar coordinates θ, r, with the origin at the crack tip; in general, we note:

$$\sigma_{ij} = \frac{K_\alpha}{\sqrt{2\pi r}} f_{ij}^{\alpha} + 0(\frac{1}{\sqrt{r}}) \tag{14}$$

The empirical formulas for the stress intensity factor for the (SENT) [52] give specimen:

$$K_I = \sigma\sqrt{\pi a}\, f\left(\frac{a}{w}\right) \tag{15}$$

$f\left(\frac{a}{w}\right)$ is a correction factor that is determined by the structure's geometry. In our case, this factor is expressed by:

$$f\left(\frac{a}{w}\right) = 1.12 - 0.231\left(\frac{a}{w}\right) + 10.55\left(\frac{a}{w}\right)^2 - 21.72\left(\frac{a}{w}\right)^3 + 30.39\left(\frac{a}{w}\right)^4 \tag{16}$$

RESULTS

Crosshead speed effect on crack propagation

A series of uniaxial tensile tests on SENT specimens at various crosshead speeds at room temperature are used to assess crack propagation behavior Fig. 6. Tab. 3 summarizes the mechanical properties. Crosshead speed has also affected toughness. As previously stated, three zones were created by dividing the curves. The conduct is initially linear at small strains, defining the elastic zone; however, as yield stress is reached, the material starts to plasticize, causing the notch to reopen. When the crosshead speed is increased, however, this value goes down. The presence of plastic deformation corresponds to the second zone. The material is softened until it reaches the minimum stress level needed for necking. Deformation continues to increase until crack propagation occurs. Even though increased crosshead speed reduces ductility, tensile strength values tend to increase. Finally, the deformation becomes macroscopically homogeneous in the third zone, and the material hardens with a higher slope before the specimen breaks. At 5mm/min crosshead speed, the

failure's strain is 40% higher than at 100mm/min. It is worth mentioning that the PVC behaves similarly at 5mm/min and 10mm/min, presumably because the crosshead speeds are so close [28]. Therefore, it can be summarized that the strain rate is a factor that controls and affects the behavior of amorphous polymers. According to the strain rate, PVC behaves in a ductile or brittle way.

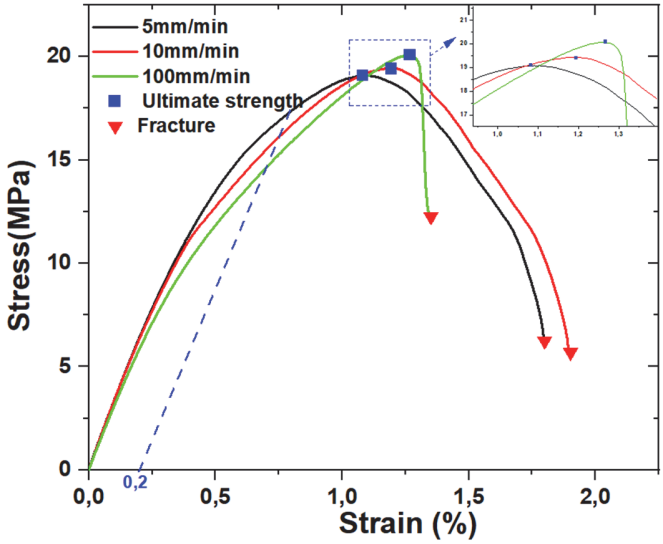

Figure 6: True stress-true strain relationships.

Mechanical characteristics	5mm/min	10mm/min	100mm/min
Yield stress (MPa)	17.27	16.03	14.7
Ultimate strength (MPa)	19.09	19.4	20.08
Rupture Elongation %	1.79	1.9	1.35

Table 3: Mechanical characteristics of PVC at different crosshead speeds

Crack length

The crack initiation and growth in PVC was caused by localized plastic deformation followed by the initiation and coalescence of microscopic voids, which will eventually break down over the formation and subsequent collapse of a crack zone in front of the crack edge.

To monitor the crack's progression. An IDS camera is used to observe the speckled samples, which is focused on the notch tips' vicinity and has a physical size of 2,4 m for each pixel. The numerical data is analyzed using the Ncorr software in Fig. 7 using a DIC technique.

After providing the crack length for all of the examined pictures at a given crosshead speed, the crack length with life fraction can be plotted in Fig. 8 to investigate the critical value of these last two.

From the graph above, we can see that the crack initially spreads in a stationary way with a linear shape between 0.15 and 0.2 of the width until it is parabolic as the crack length exceeds 0.2 of the width and until it reaches 0.5. After a short time, the crack growth accelerates and becomes uncontrollable, eventually leading to failure.

Normalizing data

Since the data from the three experiments in Fig. 8 does not show how crosshead speed affects crack propagation over the material's lifetime, we recommend that all numeric column values be normalized to standard scale values between 0 and 1. The data plot on a single curve when normalized by specimen width w and time to failure at 5mm/min crosshead speed T, as shown in Fig. 9.

Critical crack length

The critical crack length describes the transition from a stable to an unstable crack growth regime, leading to a catastrophic fracture.

Eyy using Eulerian algorithm	Eyy using Lagrangian algorithm	Time	Crack length
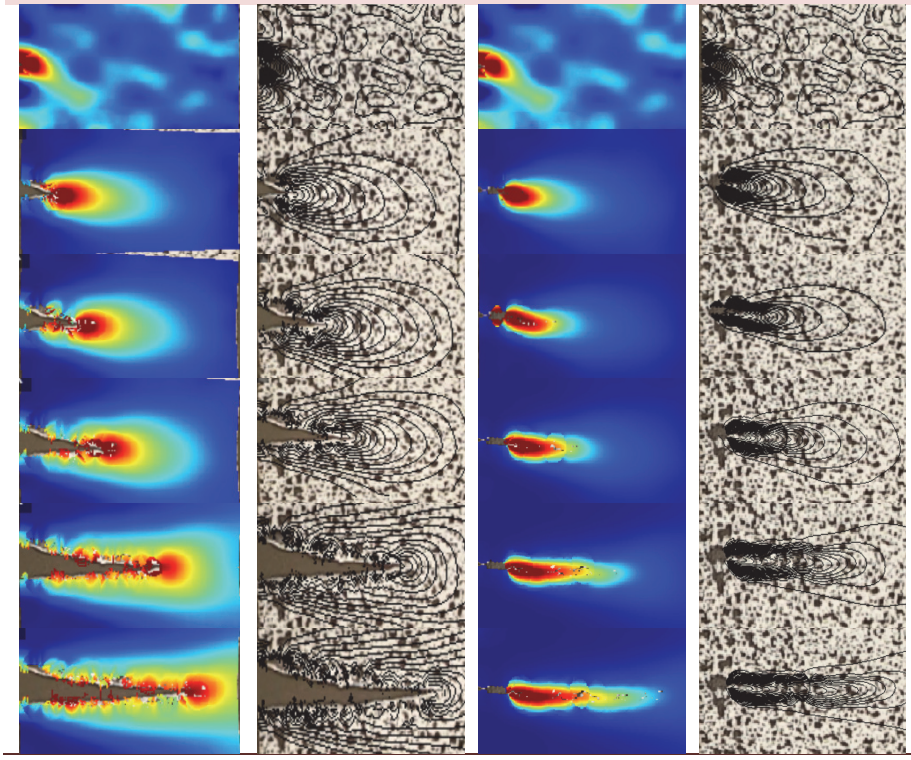		t=0s	a=3mm
		t=5,9s	a=4mm
		t=8,17s	a=6mm
		t=9.55s	a=8mm
		t=13s	a=14mm
		t=13.4s	a=16mm

Figure 7: Typical correlated axial strain fields obtained around a crack using Ncorr at 5mm/min.

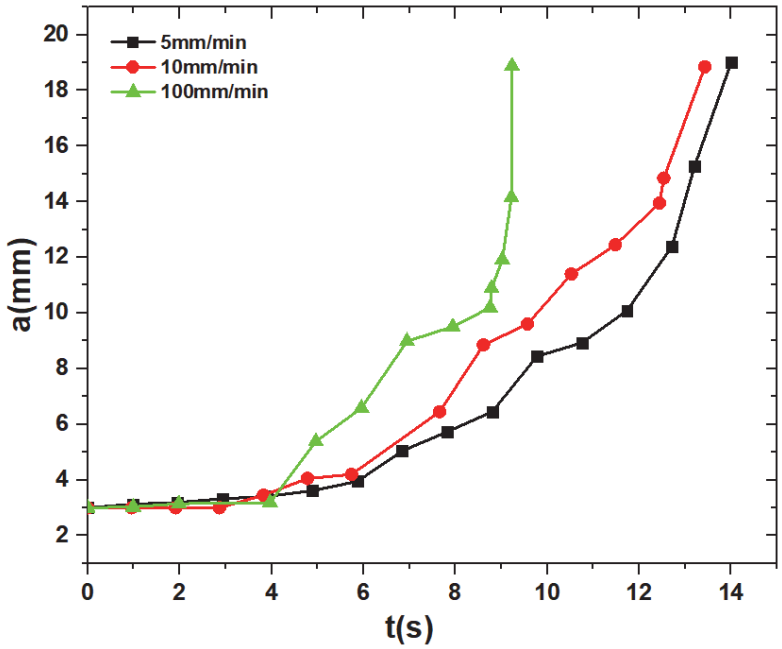

Figure 8: crack length as a function of time.

Using data from experiments, we can graphically determine the critical value of crack length and life fraction by finding the coordinates of the tangents' point of intersection with the curves. In Fig. 9, the critical life fraction is represented by the horizontal axis, while the vertical axis represents the critical crack length.

Critical crack lengths achieved are nearly constant and equal to 0.2 of the sample widths. On the other hand, the sample rapidly hits this critical value as the crosshead speed is increased, explaining the critical life fraction variance. For crosshead speeds of 100mm/min and 5mm/min, the life fraction is 31% and 42%, respectively; thus, the material at 5mm/min crosshead speed lives 35% longer than at 100mm/min.

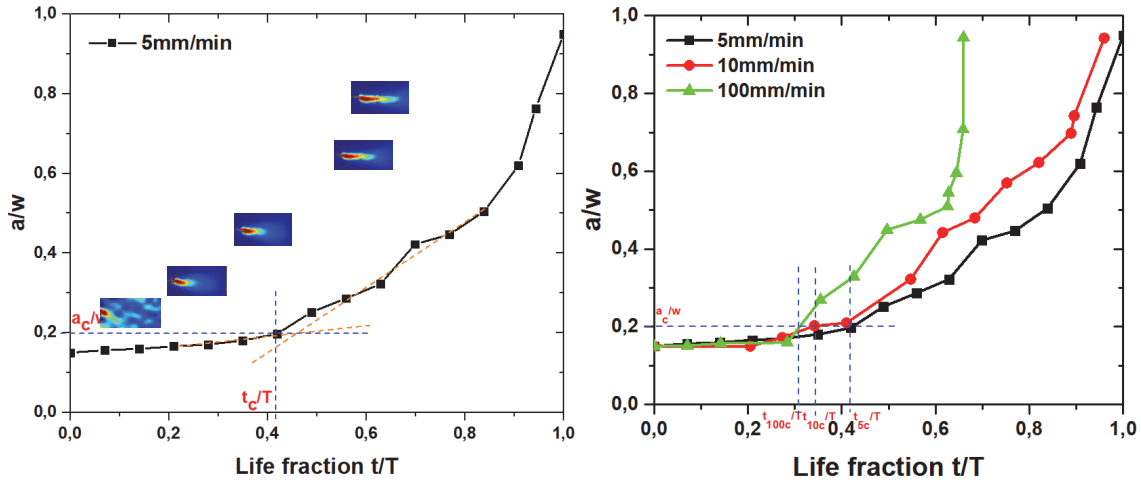

Figure 9: normalized crack length as a function of life fraction (a) at 5mm/min (b) all crosshead speed.

Stress intensity factor.

The critical stress intensity factor KIc at which crack propagation accelerates and becomes uncontrollable is fracture toughness.

To extract the critical value KIc, SIF was plotted in the crack length function using empirical Eqn. 12, Fig. 10. The KIc is the same and equals 2.6, meaning that the crosshead speed does not affect the material's toughness. We notice that the PVC acts similarly at 5mm/min and 10mm/min, likely due to the near proximity of the crosshead speeds.

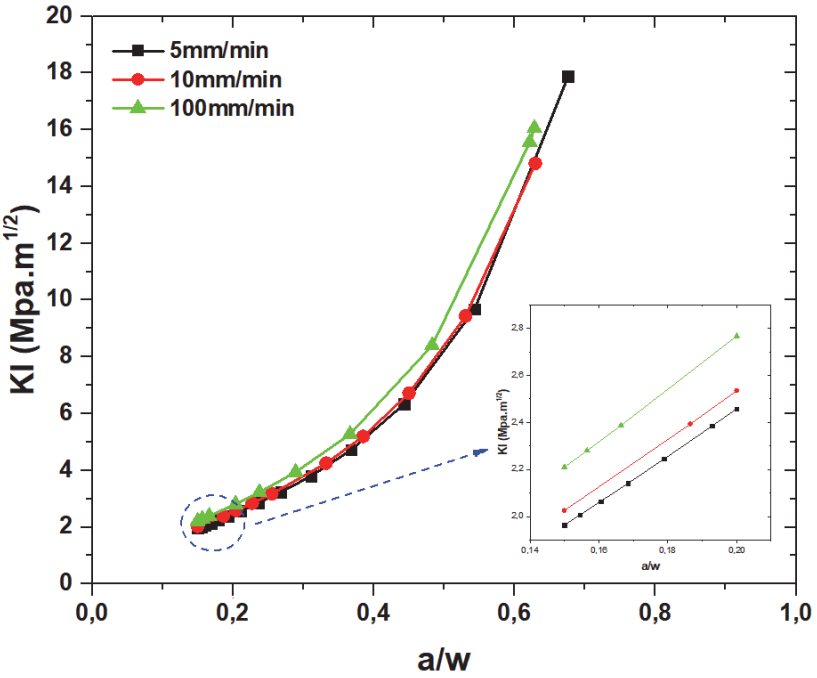

Figure 10: SIF as a function of normalized crack length.

Empirical model

Empirical models play an important role in ensuring the order and understanding of complex interrelationships between variables. By removing measurement errors, they enhance the ability to develop hypotheses and explain behaviors based on measured results.

We used a model fit that was consistent with our results to investigate the crack propagation velocity. Fig. 11 shows the evolution of crack length over time for each crosshead speed, demonstrating an exponential increase that can be expressed using an exponential function Eqn. 19. A good fitting with a correlation factor (R2>0.9) was obtained for all curves. Tab. 4 Contains the parameters α, β, and R2 of the following equation:

$$\Delta a = \alpha(e^{\beta t} - 1) \tag{19}$$

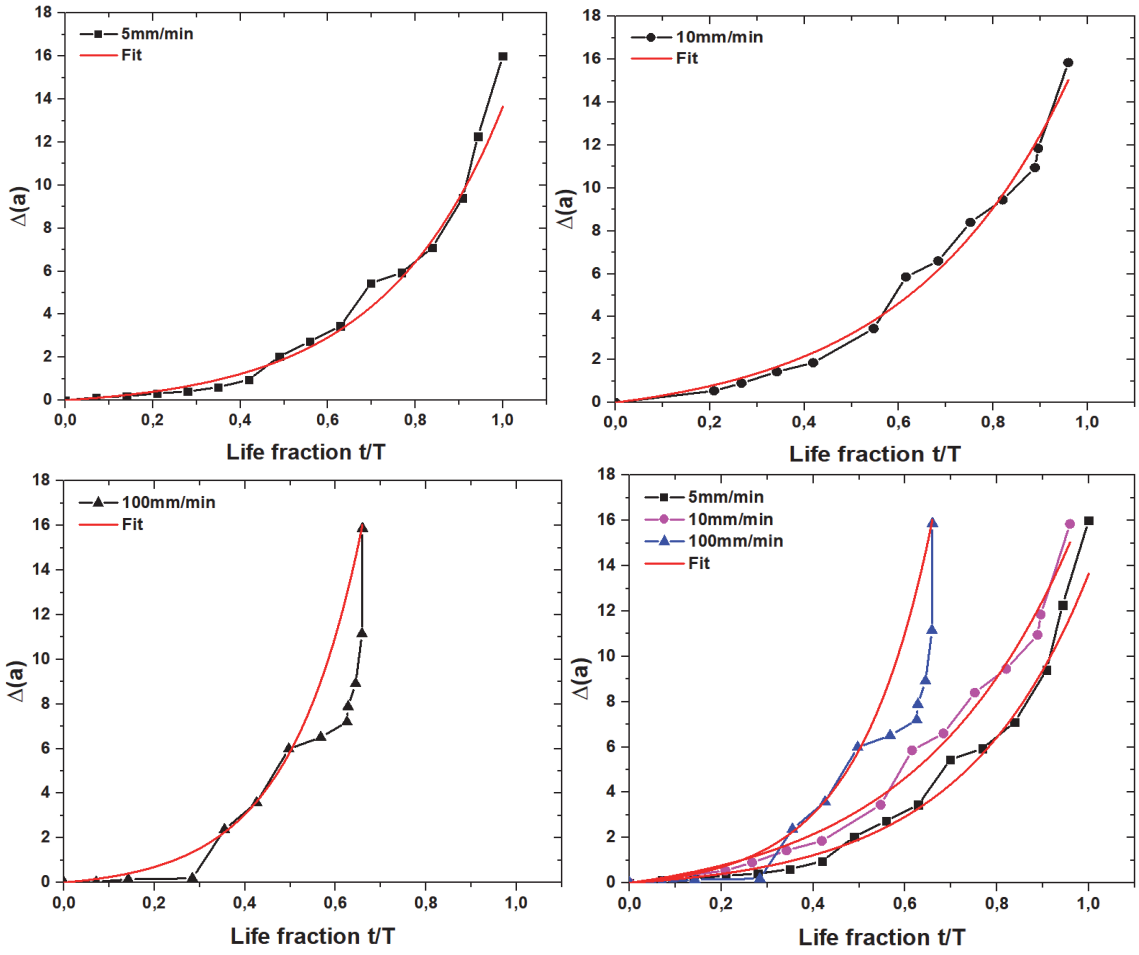

Figure 11: Model Crack length as a function of life fraction.

Crosshead speed (mm/min)	α	β	R2
5	0.29	6.09	0.99
10	0.37	3.61	0.96
100	0.97	2.92	0.98

Table 4: Parameters of the exponential model.

As seen in the table above, crosshead speed affects the parameters α and β, with α increasing and β decreasing as crosshead speed increases.

Crack growth rate

The crack velocity is determined using the model of crack length over time, and the SIF for a particular crack length is calculated and plotted as a function of the crack velocity as shown in Fig. 12.a. Following a closer study of the graphs, it was discovered that the crack growth model could be divided into three distinct stages: initiation, propagation, and failure. A stationary crack tip forms when the specimen acts in a linear elastic way in the early stages. Then comes the second phase. The crack front grows, and when the SIF exceeds the critical value, the crack begins to grow. The crack tip in this area progresses slowly at first, then lifts off. At the end of the process, the propagation becomes uncontrollable, resulting in fracture.

Furthermore, we developed a model based on experiment results, fitting the curves using Power Law Eqn. 20, with a good correlation factor (R2>0.97), which matches a linear behavior on log-log plot Fig. 12.b. with a slope of mf=0.5, which characterizes the Power law's exponent. The parameters Cf, mf, and R2 are mentioned in Tab. 4.

$$\frac{da}{dt} = C_f (\Delta K_I)^{m_f} \tag{20}$$

with

$$\Delta K_I = K_I - K_{I_0}$$

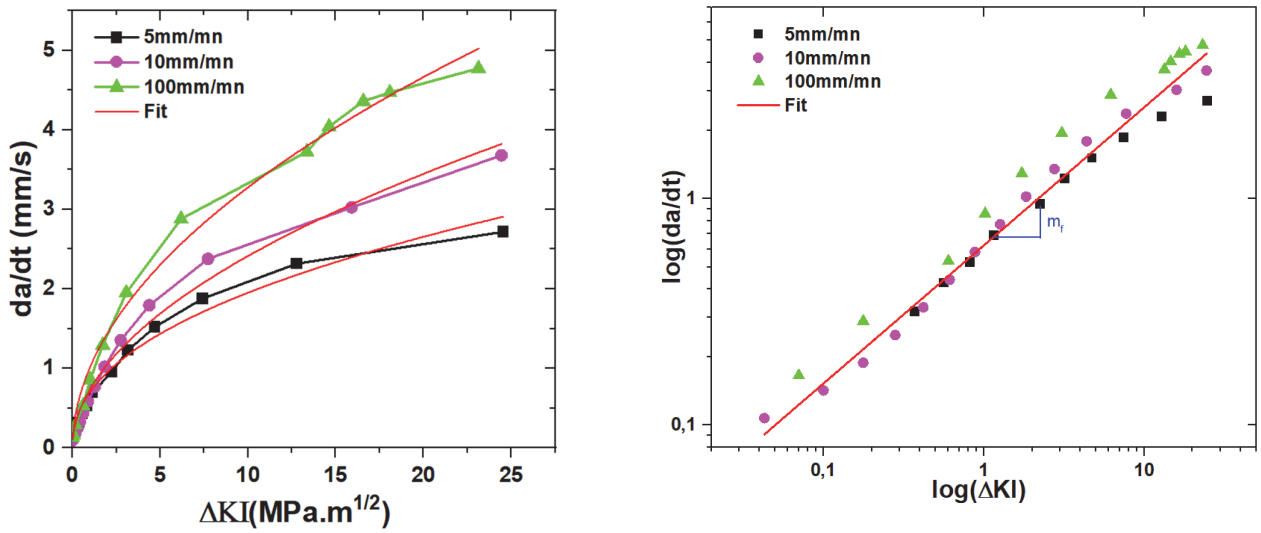

(a) (b)

Figure 12: (a). Power plot of crack growth rate; (b) logarithmic crack growth rate.

Crosshead speed (mm/min)	Cf	mf	R2
5	0.70	0.44	0.97
10	0.73	0.51	0.98
100	1.01	0.50	0.99

Table 5: Parameters of the power law model.

As shown in the table, crosshead speed affects the parameter Cf, which increased as crosshead speed increased. The exponent mf in the power law, on the other hand, is the same and equal to 0.5, meaning that the crosshead speed does not influence this parameter. This combination of findings provides some support for the conceptual premise that the exponent

mf is an intrinsic parameter of the PVC, and Cf a coefficient that describes the strain rate sensitivity, then Cf is a measure of the crack growth rate with a greater value indicating a quicker crack growth rate.

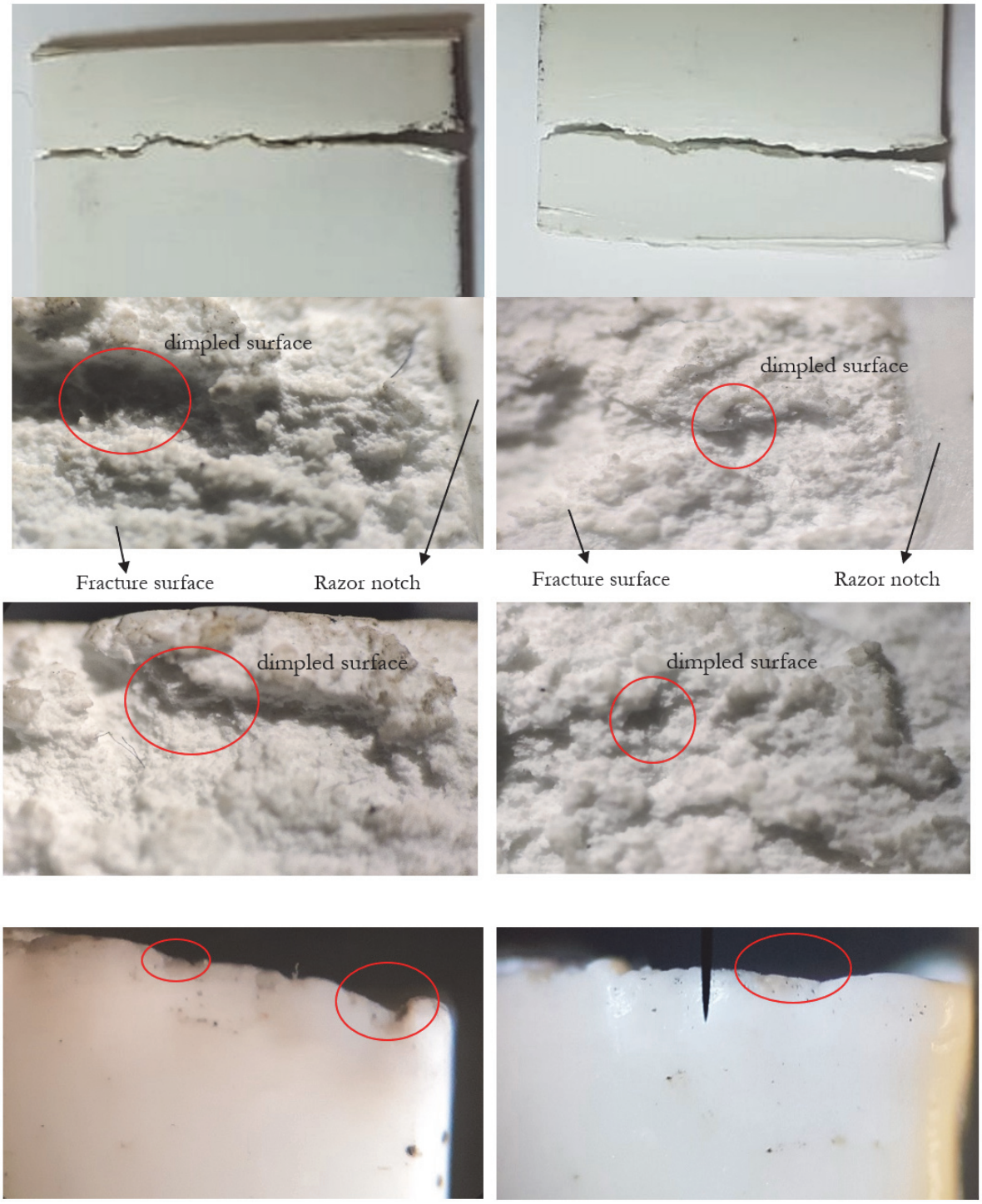

Figure 13: Fracture surfaces of PVC tensile test specimen (x4)

Optical microscopy

On a microscopic scale, the ductile failure of plastics is distinguished by a stretching of the material due to the fibrillar nature of polymers in reaction to stress. Microvoid coalescence results in ductile fracture evolution, which develops typical signatures and fracture surface patterns [53–57]. The Fig. 13 illustrates that the PVC has undergone ductile failure due to the presence of an inhomogeneous dimpled surface. When the crosshead speed is increased, however, the size of dimples and the voids becomes smaller and producing an assigned distribution of cavities with a very smooth surface texture.

CONCLUSION

PVC specimens with single-edged notches were used to investigate the effect of crosshead speed. The following are the key conclusions reached as a result of the studies conducted out during this research:

The strain rate affects the PVC behavior and the failure can be divided into two modes in crosshead speed effect tests: brittle failure at higher crosshead speeds and ductile failure at lower crosshead speeds since that, at high speed, the macromolecular chains do not have enough time to reorient themselves within the crazes causing the brittle failure.

On one hand, an exponential model is proposed to explain the crack length evolution over time based on experimental results and the DIC method, which explain the behavior of the crack propagation that spreads stationary then accelerates exponentially thus causes a sudden rupture of the sample. Further, the critical crack length is approximately constant and equal to 0.2 of the sample width at all crosshead speeds, nevertheless the sample quickly exceeds this critical value as the crosshead speed is increased, showing that crosshead speed has effect on life fraction of the material.

The critical stress intensity factor KIc remains constant at 2.6, indicating that crosshead speed has no impact on material toughness.

The crack growth rate (da/dt) and stress intensity factor correlated satisfactorily at all crosshead speeds. Therefore, to understand the behavior of the material under a power-law model was submitted to represent the crack growth rate. The prefactor parameter Cf, which increased as crosshead speed increased, is influenced by crosshead speed variance; however, the exponent mf is always equal to 0.5 and hence independent of the strain rate. As a consequence, the material's exponent mf may be thought to be an intrinsic parameter and Cf a coefficient that reflects the strain rate sensitivity.

On a microscopic scale, it has been shown that under the influence of strain rate, crazes are produced in rigid PVC, further at higher crosshead speed and at relatively high stresses, crazing and crack fibrillation are more important.

NOMENCLATURE

a	crack length
t	time
σ	nominal stress
w	width of the specimen
ν	Poisson's ratio
f(a/w)	a correction factor
r, θ	polar coordinates
KI	stress intensity factor
KIc	critical stress intensity factor
KI0	stress intensity factor at the initial crack length
N	cycle number
da/dN	fatigue crack growth rate
C	paris constant
m	paris exponent
ΔK	stress intensity factor range
da/dt	crack growth rate
Cf	power law constant
mf	power law exponent
σt	true stress
εt	true strain
F	applied load

A	actual area
L	specimen length
εyy	stress values in the loading direction
Δa	variation of crack length
R^2	correlation factor

REFERENCES

[1] Pook, L., (2000). Linear elastic fracture mechanics for engineers: theory and applications.
[2] Pook, L. P., (1983). The role of crack growth in metal fatigue. 147.
[3] Lemascon, A. Castaing, P. (1991). Failure investigation of polymer and composite material structures in the mechanical engineering industry, 5803.
[4] Smith, R., (2013). Fracture mechanics: current status, future prospects.
[5] Broek, D. (2012). The practical use of fracture mechanics.
[6] Carpinteri, A., (2012). Handbook of fatigue crack propagation in metallic structures.
[7] L.P.-T.A., (1995). Fracture Mechanics: Fundamentals and Applications—Second edition. TL Anderson. CRC Press, 2000 Corporate Blvd NW, Boca Raton, FL 33431, USA.
[8] Parton, V. (1992). Fracture mechanics: from theory to practice.
[9] Geyer, R., (2020). A Brief History of Plastics. Mare Plasticum - The Plastic Sea, pp. 31–47. DOI: 10.1007/978-3-030-38945-1_2.
[10] Babinsky, R. (2006). PVC additives: A global review. Plastics, Additives and Compounding, 8(1), pp. 38-40.
[11] Fillot, L.A., Hajji, P., Gauthier, C. and Masenelli-Varlot, K. (2007), Thermomechanical history effects on rigid PVC microstructure and impact properties, Journal of Applied Polymer Science, 104(3), pp. 2009–2017.
[12] Carrizales, C., Pelfrey, S., Rincon, R., Eubanks, T.M., Kuang, A., McClure, M.J., Bowlin, G.L. and Macossay, J. (2008). Thermal and mechanical properties of electrospun PMMA, PVC, Nylon 6, and Nylon 6,6," Polymers for Advanced Technologies, 19(2), pp. 124–130.
[13] Romo-Uribe, A., Johnson, J., Olayo, R., Romero-Guzmá, M.E., Ovalle-García, E. and Cruz-Ramos, C.A., (2008). Microstructure and dynamic mechanical analysis of extruded layered silicate PVC nanocomposites, Wiley Online Library, 19(9), pp. 1168–1176.
[14] Pita, V. J., Sampaio, E. E. M. and Monteiro, E. E., (2002). Mechanical properties evaluation of PVC/plasticizers and PVC/thermoplastic polyurethane blends from extrusion processing. Polymer Testing, 21(5), pp. 545-550.
[15] Guarrotxena, N., Martínez, G. and Millán, J., (1996). Local chain configuration dependence of the mechanisms of analogous reactions of PVC. I. A conclusive study of the microstructure evolution in SN2 nucleophilic substitution. Journal of Polymer Science Part A: Polymer Chemistry, 34(12), pp. 2387-2397.
[16] Ognedal, A. S., Clausen, A. H., Dahlen, A. and Hopperstad, O. S. (2014). Behavior of PVC and HDPE under highly triaxial stress states: An experimental and numerical study. Mechanics of Materials, 72, pp. 94-108.
[17] Bernal-Lara, T.E., Hu, Y., Summers, J., Hiltner, A. and Baer, E. (2004). Stepwise fatigue crack propagation in poly(vinyl chloride), Journal of Vinyl and Additive Technology, 10(1), pp. 5–10. DOI: 10.1002/VNL.20002.
[18] Folkman, S. and Parvez, J. (2020). PVC Pipe Cyclic Design Method, Pipelines 2020: Utility Engineering, Surveying and Multidisciplinary Topics - Proceedings of Sessions of the Pipelines 2020 Conference, pp. 304–315. DOI: 10.1061/9780784483213.034.
[19] Gugouch, F., Sandabad, S., Mouhib, N. and El Ghorba, M. (2019). Prediction of the Lifetime of the Chlorinated PVC Thermoplastic Material Subjected to Thermomechanical Tests-Tensile Test under the Influence of Temperature. In Key Engineering Materials 820, pp. 137-146. Trans Tech Publications Ltd.
[20] Saghir, F., Merah, N., Khan, Z. and Bazoune, A. (2005). Modeling the combined effects of temperature and frequency on fatigue crack growth of chlorinated polyvinyl chloride (CPVC). Journal of materials processing technology, 164, pp. 1550-1553.
[21] Majid, F., Nattaj, J. and Elghorba, M. (2016). Pressure vessels design methods using the codes, fracture mechanics and multiaxial fatigue. Frattura ed Integrità Strutturale, 10(38), 273-280. DOI: 10.3221/IGF-ESIS.38.37.
[22] Ramsteiner, F. and Armbrust, T, (2001). Fatigue crack growth in polymers, Polymer Testing, 20(3), pp. 321–327. DOI: 10.1016/S0142-9418(00)00039-8.
[23] Ding, G., Karlsson, A. M. and Santare, M. H. (2017). Numerical evaluation of fatigue crack growth in polymers based on plastically dissipated energy. International Journal of Fatigue, 94, pp. 89-96.

[24] Merah, N., Saghir, F., Khan, Z. and Bazoune, A. (2005). A study of frequency and temperature effects on fatigue crack growth resistance of CPVC. Engineering fracture mechanics, 72(11), pp. 1691-1701.
[25] Majid, F. and Elghorba, M. (2018). Continuum damage modeling through theoretical and experimental pressure limit formulas, Frattura ed Integrità Strutturale, 12(43), pp. 79–89. DOI: 10.3221/IGF-ESIS.43.05.
[26] Paris, P. and Erdogan, F. (1963). A critical analysis of crack propagation laws.
[27] Che, M., Grellmann, W. and Seidler, S. (1997). Crack resistance behavior of polyvinylchloride. Journal of applied polymer science, 64(6), pp. 1079-1090.
[28] Zekriti, N., Rhanim, R., Majid, F., Lahlou, M., Ibrahim, M. and Rhanim, H. (2020). Mode I stress intensity factors of printed and extruded specimens based on Digital Image Correlation method (DIC): case of ABS material. Procedia Structural Integrity, 28, pp. 1745-1754.
[29] Majid, F., Zekriti, N., Lahlou, M. and Mrani, B. (2020). Mechanical behavior and crack propagation of ABS 3D printed specimens. Procedia Structural Integrity, 28, pp. 1719-1726.
[30] El-Bagory, T. M. and Younan, M. Y. (2017). Crack growth behavior of pipes made from polyvinyl chloride pipe material. Journal of Pressure Vessel Technology, 139(1).
[31] Mitzenmacher, M. (2004). A brief history of generative models for power law and lognormal distributions," Internet Mathematics, 1(2), pp. 226–251. DOI: 10.1080/15427951.2004.10129088.
[32] Clauset, A., Shalizi, C.R. and Newman, M.E.J. (2009). Power-law distributions in empirical data, SIAM Review, 51(4), pp. 661–703. DOI: 10.1137/070710111.
[33] Kim, M., Park, T. Y. and Hong, S. (2021). Experimental determination of the plastic deformation and fracture behavior of polypropylene composites under various strain rates. Polymer Testing, 93, 107010.
[34] J Djouda, J. M., Bouaziz, M. A., Zouaoui, M., Rambaudon, M., Gardan, J., Recho, N. and Crépin, J. (2020). Experimental approach for microscale mechanical characterization of polymeric structured materials obtained by additive manufacturing. Polymer Testing, 89, 106634.
[35] Livieri, P. (2008). Use of J-integral to predict static failures in sharp V-notches and rounded U-notches. Engineering fracture mechanics, 75(7), pp. 1779-1793.
[36] Sutton, M., Orteu, J. and Schreier, H. (2009). Image correlation for shape, motion and deformation measurements: basic concepts, theory and applications.
[37] Sutton, M. A., Wolters, W. J., Peters, W. H., Ranson, W. F. and McNeill, S. R. (1983). Determination of displacements using an improved digital correlation method. Image and vision computing, 1(3), pp. 133-139.
[38] Chu, T. C., Ranson, W. F. and Sutton, M. A. (1985). Applications of digital-image-correlation techniques to experimental mechanics. Experimental mechanics, 25(3), 232-244.
[39] Pan, B., Qian, K., Xie, H. and Asundi, A. (2009). Two-dimensional digital image correlation for in-plane displacement and strain measurement: a review. Measurement science and technology, 20(6), 062001.
[40] Liu, M., Guo, J., Li, Z., Hui, C. Y. and Zehnder, A. T. (2019). Crack propagation in a PVA dual-crosslink hydrogel: Crack tip fields measured using digital image correlation. Mechanics of Materials, 138, 103158.
[41] Pan, B., Wang, Z. and Lu, Z. (2010). Genuine full-field deformation measurement of an object with complex shape using reliability-guided digital image correlation. Optics express, 18(2), pp. 1011-1023.
[42] Pan, B. and Li, K. (2011). A fast digital image correlation method for deformation measurement. Optics and Lasers in Engineering, 49(7), pp. 841-847.
[43] Pan, B., Asundi, A., Xie, H. and Gao, J. (2009). Digital image correlation using iterative least squares and pointwise least squares for displacement field and strain field measurements. Optics and Lasers in Engineering, 47(7-8), pp. 865-874.
[44] Pan, B., Li, K. and Tong, W. (2013). Fast, Robust and Accurate Digital Image Correlation Calculation Without Redundant Computations, Experimental Mechanics, 53(7), pp. 1277–1289. DOI: 10.1007/S11340-013-9717-6.
[45] Helm, J. D., McNeill, S. R. and Sutton, M. A. (1996). Improved three-dimensional image correlation for surface displacement measurement. Optical Engineering, 35(7), pp. 1911-1920.
[46] Ab Ghani, A. F., Ali, M. B., Dhar Malingam, S. and Mahmud, J. (2016). Digital image correlation (DIC) technique in measuring strain using opensource platform Ncorr. Journal of Advanced Research in Applied Mechanics, 26(1), pp. 10-21.
[47] Harilal, R. (2014). Adaptation of open source 2D DIC software Ncorr for solid mechanics applications.
[48] Blaber, J., Adair, B. and Antoniou, A. (2015). Ncorr: Open-Source 2D Digital Image Correlation Matlab Software, Experimental Mechanics, 55(6), pp. 1105–1122.
[49] Irwin, G.R. and Wells, A.A. (1965). A continuum-mechanics view of crack propagation, Metallurgical Reviews, 10(1), pp. 223–270. DOI: 10.1179/MTLR.1965.10.1.223.

[50] Irwin, G.R. (1962). Crack-Extension Force for a Part-Through Crack in a Plate, Journal of Applied Mechanics, 29(4), pp. 651–654. DOI: 10.1115/1.3640649.
[51] Weertman, J. (1978). Fracture mechanics: A unified view for Griffith-Irwin-Orowan cracks. Acta Metallurgica, 26(11), pp. 1731-1738.
[52] Miannay, D. (1972). Notions élémentaires sur la rupture des métaux. II.–La mécanique de la rupture. Matériaux and Techniques, 60(2), pp. 51-53.
[53] Frontini, P., Bernal, C.R., Frontini, P.M., Sforza, M. and Bibb, M.A. (1995). Microstructure, deformation and fracture behavior of commercial ABS resins, Wiley Online Library, 58(1), pp. 1–10. DOI: 10.1002/app.1995.070580101.
[54] Pantazopoulos, G. A. (2019). A short review on fracture mechanisms of mechanical components operated under industrial process conditions: Fractographic analysis and selected prevention strategies. Metals, 9(2), 148.
[55] Vu-Khanh, T. and De Charentenay, F. X. (1985). Mechanics and mechanisms of impact fracture in semi-ductile polymers. Polymer Engineering and Science, 25(13), pp. 841-850. DOI: 10.1002/PEN.760251309.
[56] Gryshchuk, O., Jost, N. and Karger-Kocsis, J. (2002). Toughening of vinylester-urethane hybrid resins through functionalized polymers, Journal of Applied Polymer Science, 84(3), pp. 672–680. DOI: 10.1002/APP.10392.
[57] Toda, H., Tomizato, F., Harasaki, R., Seo, D., Kobayashi, M., Takeuchi, A. and Uesugi, K. (2016). 3D fracture behaviours in dual-phase stainless steel. ISIJ international, 56(5), pp. 883-892.